nature nanotechnology

LETTERS

PUBLISHED ONLINE: 26 OCTOBER 2014 | DOI: 10.1038/NNANO.2014.234

Nanotube mechanical resonators with quality factors of up to 5 million

J. Moser[1], A. Eichler[1†], J. Güttinger[1], M. I. Dykman[2] and A. Bachtold[1*]

Carbon nanotube mechanical resonators have attracted considerable interest because of their small mass, the high quality of their surfaces, and the pristine electronic states they host[1–4]. However, their small dimensions result in fragile vibrational states that are difficult to measure. Here, we observe quality factors Q as high as 5×10^6 in ultra-clean nanotube resonators at a cryostat temperature of 30 mK, where we define Q as the ratio of the resonant frequency over the linewidth. Measuring such high quality factors requires the use of an ultra-low-noise method to rapidly detect minuscule vibrations, as well as careful reduction of the noise of the electrostatic environment. We observe that the measured quality factors fluctuate because of fluctuations of the resonant frequency. We measure record-high quality factors, which are comparable to the highest Q values reported in mechanical resonators of much larger size[5,6], a remarkable result considering that reducing the size of resonators is usually concomitant with decreasing quality factors. The combination of ultra-low mass and very large Q offers new opportunities for ultra-sensitive detection schemes and quantum optomechanical experiments.

In recent years, endeavours to boost quality factors in nano- and micromechanical resonators have been stimulated by the need to develop innovative approaches to sensing[7], signal processing[8] and quantum physics[9]. Strategies to enhance quality factors have proceeded along three main routes. First, the quality of the host material has been improved. To this end, new materials have been employed, such as high-tensile-stress silicon nitride membranes[5,10] and single-crystal diamond films[11]. In addition, surface friction has been lowered by optimizing fabrication processes and reducing contamination[12]. Second, schemes to isolate the resonator from its surrounding environment have been developed, based on new resonator layouts[13,14] and on optical trapping of thin membranes and levitated particles[15,16]. Third, and most straightforwardly, Q-factors have been improved by operating resonators at cryogenic temperatures[17].

Schemes to enhance Q-factors in nanotube resonators have focused on reducing contamination by growing ultra-clean nanotubes and by cooling resonators down to millikelvin temperatures[2]. Even though Q-factors, measured from the linewidth of driven resonances, have been improved up to $\sim 1.5 \times 10^5$, they are still much lower than the values routinely obtained with larger resonators fabricated from bulk materials using top-down techniques[6]. This result is somewhat disappointing, because the high crystallinity of nanotubes and their lack of dangling bonds at the surface are expected to minimize the surface friction that limits the Q-factor in some nanomechanical systems[18].

Here, we find that the actual values of the Q-factors can be significantly higher than hitherto appreciated, but that revealing these values requires improving the measurement technique. Namely, the dynamics of the nanotube has to be captured in a regime of vanishingly small displacement in order to minimize nonlinear effects. In addition, noise from the electrostatic environment has to be reduced as much as possible. Indeed, owing to the ultrasmall mass of nanotubes, this electrostatic noise affects the frequency of the nanotube resonator enormously and broadens the

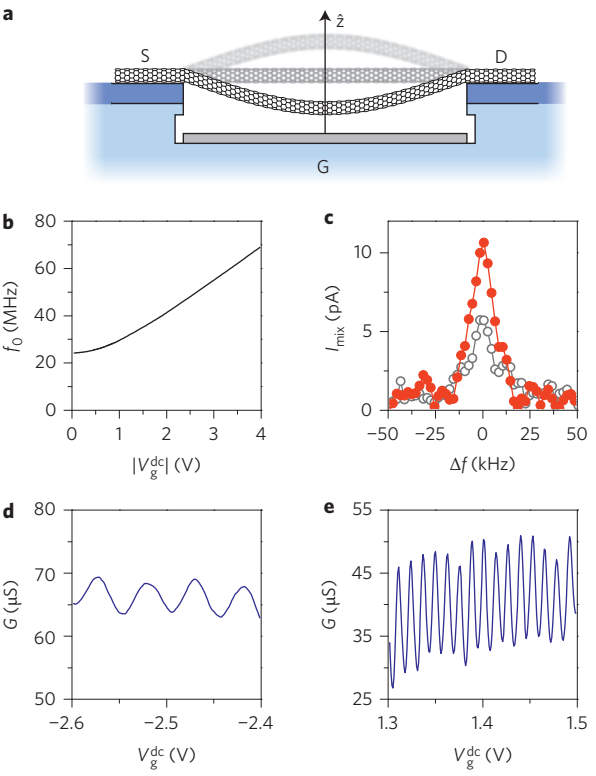

Figure 1 | Carbon nanotube mechanical resonator. a, Schematic of device. The nanotube is contacted by source (S) and drain (D) electrodes, and is suspended over a gate electrode (G). The trench has a width of 1.8 μm and a depth of ~ 350 nm. **b**, Resonant frequency f_0 as a function of gate voltage $|V_g^{dc}|$ for the lowest-lying mechanical mode. **c**, Mixing current I_{mix} as a function of drive frequency Δf (measured from $f_0 = 44.1$ MHz), using the FM technique. $V_g^{dc} = -2.2$ V. Two different driving voltage amplitudes were used: 13 μV (filled red circles) and 8 μV (open circles). A lock-in amplifier with a time constant of 300 ms was used. In the FM technique, the Q-factor is extracted from the width of the foot of the resonance[20,21], yielding $Q \approx 1{,}700$. **d**,**e**, Conductance G as a function of V_g^{dc}, in the Fabry–Perot regime (**d**) and in the Coulomb blockade regime (**e**). The full $G(V_g^{dc})$ trace is shown in Supplementary Section I.

[1]ICFO–Institut de Ciencies Fotoniques, Mediterranean Technology Park, 08860 Castelldefels (Barcelona), Spain, [2]Department of Physics and Astronomy, Michigan State University, East Lansing, Michigan 48824, USA; †Present address: Department of Physics, ETH Zurich, Schafmattstrasse 16, 8093 Zurich, Switzerland. *e-mail: adrian.bachtold@icfo.es

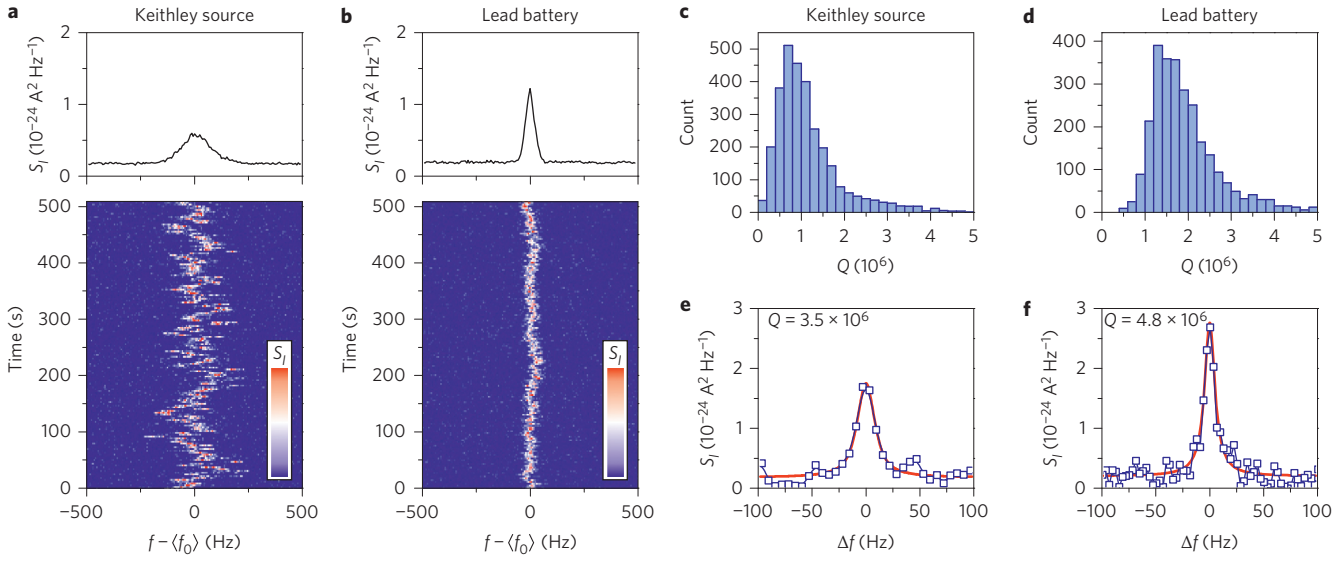

Figure 2 | Fluctuations of the *Q*-factor and resonant frequency. a, Bottom: Power spectra of current fluctuations $S_I(f - \langle f_0 \rangle)$ acquired successively in time, using a commercial d.c. voltage source (Keithley) to supply the gate voltage ($V_g^{dc} = -3.037$ V). For each of these spectra the measurement time was 3.2 s. Top: Resonance obtained by averaging all spectra. **b**, Same experiment as in **a**, this time using a lead battery to supply the gate voltage. Scale bars: power spectral density $S_I = 0.15 \times 10^{-24}$ A^2 Hz^{-1} (blue) to $S_I = 2.50 \times 10^{-24}$ A^2 Hz^{-1} (red). **c**,**d**, Histograms of *Q*-factor using the Keithley source (**c**) and the lead battery (**d**), constructed from 3,000 power spectra acquired with the same settings as in **a**,**b**. **e**,**f**, Examples of high *Q* resonances obtained with the Keithley source (**e**) and the lead battery (**f**). Red curves are fits to Lorentzian functions. For all panels, $\langle f_0 \rangle = 55.6$ MHz is the time-averaged resonant frequency.

mechanical linewidth. All these experimental requirements make it challenging to unmask the instrinsic *Q*-factor. Progress in measuring ring-down with nanotubes has been made[19], but it has not revealed higher *Q*-factor values. One reason for this might be that the large displacements in those measurements lead to sizeable nonlinearities.

The geometry of our device, as well as its characterization, are presented in Fig. 1. The nanotube is contacted by source (S) and drain (D) electrodes, and is suspended over a trench; at the bottom of the trench is a local gate electrode (Fig. 1a). In this scheme, the ultra-clean nanotube was grown by chemical vapour deposition in the last step of the fabrication process of the resonator, making it free of fabrication residues. The device was cooled to 30 mK, at which temperature all the data presented here were taken. We identified the lowest-lying flexural mode of the resonator using the frequency-modulated (FM) mixing technique[20,21], and studied its dependence on gate voltage $|V_g^{dc}|$ (Fig. 1b). Figure 1c presents resonance lineshapes in response to oscillating electrostatic forces (measured with the FM technique), which yield $Q = 1{,}700$. The voltages used to produce these driving forces were kept low so that the resonance lineshapes were just above the noise floor.

An ultra-sensitive detection method (described in ref. 22) was used to capture the tiny amplitude of the thermal vibrations at 30 mK. In contrast to the FM technique, the resonator was not driven by an oscillating force. Displacement fluctuations were transduced into current fluctuations, from which power spectra S_I were measured (see Methods). We operated the resonator within the electron Fabry–Perot regime (Fig. 1d), where the effect of electron transport on mechanical vibrations is less pronounced than in the Coulomb blockade regime (Fig. 1e)[2–4,23]. A typical resonance lineshape, obtained by averaging power spectra for ~512 s, is shown in the upper panel of Fig. 2a. The corresponding *Q*-factor is $Q \approx 4 \times 10^5$ for a resonant frequency $f_0 = 55.6$ MHz. Remarkably, such a *Q*-factor is 200 times higher than that measured with the FM mixing technique (Fig. 1c).

We find that both the *Q*-factor and f_0 fluctuate in time. To show this, spectra obtained over a measurement time $\tau = 3.2$ s were acquired successively, using either a commercial Keithley source or a simple lead battery to supply V_g^{dc} (see colour plots of S_I as a function of frequency and time in Fig. 2a,b). Frequency fluctuations with the Keithley source are larger than with the lead battery. The *Q*-factor also fluctuates, and its distribution is broad and asymmetric (Fig. 2c,d). On average, *Q*-factors are higher with the lead battery than with the Keithley source. Although fluctuations in f_0 have been observed in high-*Q* mechanical resonators[24–26], fluctuations in the measured *Q*-factor have not been discussed thus far. We show in the following that both fluctuations are closely related.

The averaged *Q*-factor decreases with measurement time (Fig. 3a). Once the measurement time is set, the *Q*-factor does not reveal any marked dependence on the amplitude V_{sd}^{ac} of the oscillating source–drain bias used to read out current fluctuations (Fig. 3b). This shows that V_{sd}^{ac} does not affect the measured motion of the resonator. For example, if the resonator were to heat up due to Joule heating, the *Q*-factor would decrease as V_{sd}^{ac} increases, and if the resonator were to self-oscillate, the *Q*-factor would vary as V_{sd}^{ac} increases. Neither the *Q*-factor nor f_0 changes as V_g^{dc} is swept through a conductance oscillation (Supplementary Section VI). This confirms that the effect of electron transport on the vibrations is weak. This is crucial to our experiment, because Coulomb blockade would reduce the *Q*-factor[2–4,23].

The observed frequency fluctuations are associated with the electrostatic noise of the environment. In the case of the Keithley source, frequency fluctuations are traced back to the voltage fluctuations of the source itself as a result of the strong gate voltage dependence of f_0. To show this, we transformed voltage fluctuations into Allan deviation σ_A using the f_0-to-V_g^{dc} conversion factor measured in Fig. 1b, $\sim 1.4 \times 10^7$ Hz V^{-1} (see Methods). In Fig. 3c we find that the measured Allan deviation of the resonant frequency of the nanotube (green open circles) coincides with the Allan deviation expected from the gate voltage fluctuations generated by the source (blue trace). The frequency noise is of $1/f$-type (pink noise), because σ_A is essentially constant as a function of measurement time τ. By contrast, the lead battery is stable enough that it does not significantly affect f_0. The Allan deviation expected from the voltage fluctuations of the lead battery is smaller than $\sigma_A(\tau)$ measured with the nanotube resonator (Fig. 3d). The origin of the

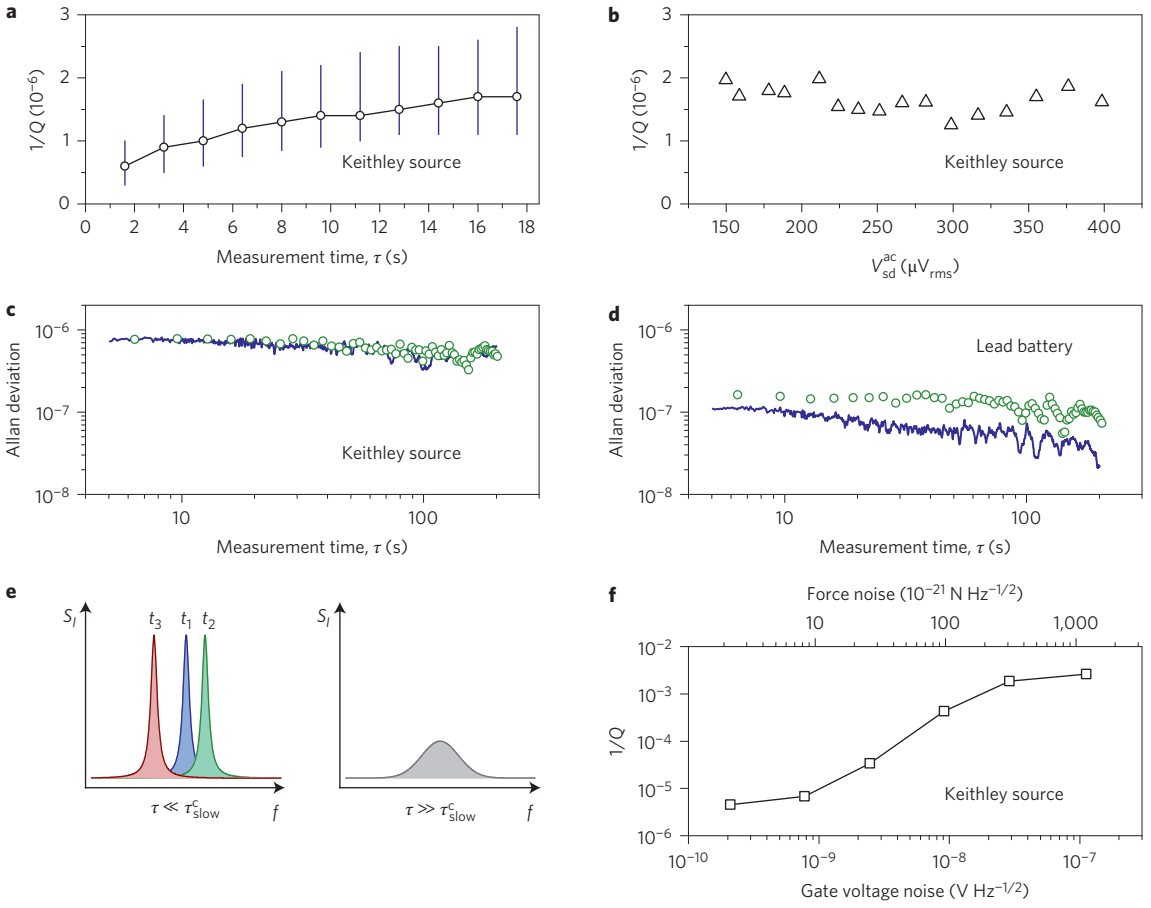

Figure 3 | Characterization of the *Q*-factor and of the fluctuations in f_0. **a**, $1/Q$ as a function of measurement time τ, using the Keithley source. For each measurement time, 300 power spectra were acquired and a histogram of $1/Q$ was built. Circles denote $1/Q$ at the maximum of the histograms and bars represent the full-width at half-maximum of the histograms. The resonant frequency is $f_0 = 55.6$ MHz for **a**–**d**. **b**, $1/Q$ as a function of V_{sd}^{ac} for $\tau = 16$ s. **c**,**d**, Allan deviation of f_0 as a function of τ with the Keithley source (**c**) and with the lead battery (**d**). Green circles indicate measured resonant frequencies and blue traces represent resonant frequencies estimated from gate voltage fluctuations. **e**, Schematic of resonance lineshapes for short (left) and long (right) measurement times τ compared to the characteristic time of the slow frequency noise τ_{slow}^{c}. $t_{1,2,3}$ are three successive instants. **f**, $1/Q$ as a function of added gate voltage noise at $V_g^{dc} = -2.2$ V ($f_0 = 44.1$ MHz) for $\tau = 16$ s. The gate voltage noise was applied using the Johnson–Nyquist noise of a 50 Ω resistor at room temperature amplified by different gains. It creates a white electrostatic force noise between the nanotube and the gate (top axis).

observed frequency fluctuations with the lead battery is not clear. Because σ_A remains constant as a function of τ ($1/f$ noise), f_0 fluctuations might be related to two-level systems such as charge fluctuators in the gate dielectric.

The Q-factor is also affected by the electrostatic noise of the environment. This can be inferred from a comparison of Fig. 2a and b. Larger fluctuations of the resonant frequency (lower panels) result in a larger resonance linewidth (upper panels), and hence a lower Q-factor.

The fluctuations of the quality factor, the asymmetry of its distribution and its dependence on measurement time are all attributed to the fluctuations of the resonant frequency. To show this, we separated this frequency noise into a slow part and a fast part on the scale of the ring-down time (see Methods and Supplementary Section X). For a measurement time τ that is short compared to the characteristic timescale of the slow frequency noise τ_{slow}^{c}, resonances have a Lorentzian lineshape with a constant width $2\tilde{\Gamma}$ and a resonant frequency that fluctuates from one measurement to the next. For $\tau \gg \tau_{slow}^{c}$, resonances are broadened by the time average of many such Lorentzians, resulting in non-Lorentzian lineshapes (Fig. 3e). For $\tau \approx \tau_{slow}^{c}$, linewidths are larger than $2\tilde{\Gamma}$, and fluctuate from one measurement to the next. On increasing τ, linewidths tend to increase because the resonator has time to explore a larger frequency range. The distribution of linewidths is asymmetric because linewidths have a fixed lower bound given by $2\tilde{\Gamma}$ (Supplementary Section X).

Figure 2e,f presents two high-Q resonance lineshapes (obtained with both gate voltage sources), which give values of $Q = 3.5 \times 10^6$ (Keithley source) and $Q = 4.8 \times 10^6$ (lead battery). We verified that the areas of the resonances in the S_I spectra in Fig. 2e,f are equal (within 10%) to the areas of the averaged resonances in Fig. 2a,b. This confirms that these sharp resonances do capture the dynamics of the nanotube, in spite of the relatively low number of measurement points dictated by the short measurement time. A slightly lower quality factor is obtained in an additional device, also operated in the Fabry–Perot regime (Supplementary Section IX), confirming the robustness of high-Q resonances. These Q-factors are comparable to the highest values measured in large micromechanical resonators[5]. Yet, they may still be limited by the measurement and may not have reached the intrinsic Q-factor of nanotube resonators, defined as f_0 multiplied by the small-amplitude ring-down time (the ring-down time is not known, but it is smaller than τ; Supplementary Section X).

The large quality factors observed here are associated with the small amplitude of the nanotube vibrations. Using the equipartition theorem, the mode temperature is obtained as $T = 44 \pm 10$ mK,

which corresponds to a phonon population of $n = k_B T/hf_0 = 16 \pm 4$, where k_B is the Boltzmann constant and h is Planck's constant (Supplementary Section V). In this estimate, we use the areas of the resonances in Fig. 2, which are all equal within 10%. From the temperature, we calculate that the variance of displacement is $\sim(35\ \text{pm})^2$.

Larger displacements translate into lower Q-factors. This is illustrated in Fig. 3f, where a white voltage noise is applied to the gate electrode to enhance the displacement. Possible origins of this behaviour could be associated with nonlinear damping forces, which result in a mechanical linewidth that depends on the amplitude of motion and the spectral broadening of the resonance, which is induced by the combination of nonlinear conservative forces and displacement fluctuations[21,27–29]. Note that the applied voltage noise also induces fluctuations in f_0, but their contribution to the measured resonance linewidth is negligible (Supplementary Section VII). The temperature dependence of the Q-factor could not be measured in our current measurement set-up.

The giant quality factors and the associated weak fluctuations of f_0 hold promise for diverse sensing experiments. The limit to force sensing is ultimately set by the force noise $S_f = 8\pi M k_B T f_0/Q$ (ref. 22). Using $M = 4.4 \times 10^{-21}$ kg, $Q = 4.8 \times 10^6$ and $T \approx 44$ mK, we obtain $\sqrt{S_f} \approx 1 \times 10^{-21}\ \text{N Hz}^{-1/2}$, which is lower than what has been achieved with mechanical resonators to date[22]. The sensitivity of mass sensing and force gradient detection is given by the Allan deviation of frequency fluctuations ($\delta f_0 \approx 8$ Hz for $\tau \approx 6$ s) in Fig. 3d obtained with the lead battery. The latter translates into a mass resolution of $\delta M = 2M \times \delta f_0/f_0 \approx 1 \times 10^{-27}$ kg, which is as good as the best estimates on record[1]. We extract a force gradient resolution of $8\pi^2 M f_0 \delta f_0 \approx 1 \times 10^{-10}\ \text{N m}^{-1}$, which compares favourably with the best values reported thus far[30].

Nanotube resonators are relevant candidates for exploring the quantum regime of nanomechanics. Their low mass leads to large zero-point motion, $\sqrt{\hbar/(4\pi f_0 M)} \approx 6$ pm and allows the coupling to other quantum systems to be enhanced. High Q-factors are necessary for the quantum manipulation of mechanical states. In an experiment where the resonator is cooled to the ground state with passive feedback, the lifetime of the ground state is $\tau_{ph} = \hbar Q/k_B T \approx 1 \times 10^{-3}$ s (for $k_B T > hf_0$) using $T \approx 44$ mK and assuming that $Q = 4.5 \times 10^6$ is related to the ring-down time. Our nanotube resonator demonstrates $Qf_0 = 3 \times 10^{14}$ Hz, which compares well with the highest values measured to date in nano- and micromechanical resonators[14,31].

Overall, our work shows that the Q-factor of ultra-clean nanotube resonators can reach very high values, provided that the resonators are cooled to a low enough temperature for nonlinear effects to be negligible, that slow frequency noise is reduced, that measurement times are short and that the effect of coupling between vibrations and Coulomb blockade is suppressed. The unique combination of ultra-low mass and giant quality factors offers new opportunities for ultra-sensitive detection schemes and optomechanical experiments in the quantum regime.

Methods

Detecting thermal vibrations. We used an ultra-sensitive detection method that allowed us to capture the tiny amplitude of the thermal vibrations in a dilution refrigerator cooled to 30 mK. Displacement fluctuations δz in direction $\hat{z}$ normal to the gate were transduced into conductance fluctuations $\delta G = \frac{dG}{dV_g} V_g^{dc} \frac{C_g'}{C_g} \delta z$, where C_g is the capacitance between the nanotube and the gate, and $C_g' = dC_g/dz$ (for the estimation of C_g', see Supplementary Section II). Large transduced signals require a large transconductance dG/dV_g. The largest transconductance was obtained in the Coulomb blockade regime, for $V_g^{dc} > 0$ (Fig. 1e), as is usually observed in ultra-clean suspended nanotubes[32]. However, Coulomb blockade reduces Q-factors, because it amplifies the coupling between electron transport and mechanical vibrations[2–4,23]. For this reason, we operated the resonator within the Fabry–Perot regime, realized for $V_g^{dc} < 0$, even though dG/dV_g is lower (Fig. 1d). In this regime, oscillations in conductance originate from quantum interferences of electronic waves, and the effect of the coupling between vibrations and Coulomb blockade is weaker. The tiny conductance fluctuations δG are parametrically downconverted into low-frequency current fluctuations δI by applying a small oscillating voltage of amplitude V_{sd}^{ac} across source and drain, at a frequency f_{sd} shifted by ~10 kHz from the mechanical resonant frequency f_0. Power spectra S_I of fluctuations δI were measured at frequencies $|f_{sd} - f_0| \approx 10$ kHz with a cross-correlation technique using a vector signal analyser[22].

Allan deviation. We calculate the Allan deviation σ_A as

$$\sigma_A^2(\tau) = \frac{1}{2(N-1)} \sum_{i=1}^{N-1} \left(\frac{\langle f_{i+1} \rangle_\tau - \langle f_i \rangle_\tau}{\langle f_0 \rangle} \right)^2$$

where $\langle f_{i+1} \rangle_\tau$ and $\langle f_i \rangle_\tau$ are two subsequent measurements of f_0 averaged over the measurement time τ, N is the number of averaged frequency measurements and $\langle f_0 \rangle$ is the average of f_0 over the whole measurement[33]. We define f_0 as the frequency for which S_I is largest.

Power spectrum of displacement and frequency noise. We separated the frequency noise into a slow part and a fast part on the scale of the ring-down time. The power spectrum of displacement S_q (which is proportional to S_I) as a function of angular frequency $\omega = 2\pi f$ is given by

$$S_q(\omega) = \frac{k_B T}{M\omega_0^2} \frac{1}{\tau} \int_0^\tau dt \frac{\tilde{\Gamma}}{\tilde{\Gamma}^2 + [\omega - \tilde{\omega}_0 - \xi_{slow}(t)]^2}$$

where k_B is the Boltzmann constant, T is the mode temperature, t is the time and M is the modal mass. $\tilde{\Gamma}$ is the sum of the reciprocal ring-down time and of the broadening due to fast frequency noise, $\tilde{\omega}_0$ is the resonant angular frequency renormalized by the fast frequency noise and ξ_{slow} is the slow part of the frequency noise (Supplementary Section X). The area $\int_0^\infty S_q(\omega) d\omega = \pi k_B T/M\omega_0^2$ is given by the equipartition theorem, so it is independent of frequency noise.

Received 17 February 2014; accepted 13 September 2014; published online 26 October 2014

References

1. Chaste, J. *et al.* A nanomechanical mass sensor with yoctogram resolution. *Nature Nanotech.* **7,** 301–304 (2012).
2. Steele, G. A. *et al.* Strong coupling between single-electron tunneling and nanomechanical motion. *Science* **325,** 1103–1107 (2009).
3. Lassagne, B., Tarakanov, Y., Kinaret, J., Garcia-Sanchez, D. & Bachtold, A. Coupling mechanics to charge transport in carbon nanotube mechanical resonators. *Science* **325,** 1107–1110 (2009).
4. Benyamini, A., Hamo, A., Viola Kusminskiy, S., von Oppen, F. & Ilani, S. Real-space tailoring of the electron–phonon coupling in ultra-clean nanotube mechanical resonators. *Nature Phys.* **10,** 151–156 (2014).
5. Adiga, V. P. *et al.* Approaching intrinsic performance in ultra-thin silicon nitride drum resonators. *J. Appl. Phys.* **112,** 4323 (2012).
6. Poot, M. & van der Zant, H. S. J. Mechanical systems in the quantum regime. *Phys. Rep.* **511,** 273–335 (2012).
7. Li, M., Tang, H. X. & Roukes, M. L. Ultra-sensitive NEMS-based cantilevers for sensing, scanned probe and very high-frequency applications. *Nature Nanotech.* **2,** 114–120 (2007).
8. Mahboob, I. & Yamaguchi, H. Bit storage and bit flip operations in an electromechanical oscillator. *Nature Nanotech.* **3,** 275–279 (2008).
9. Aspelmeyer, M., Meystre, P. & Schwab, K. Quantum optomechanics. *Phys. Today* **65,** 29 (July, 2012).
10. Rieger, J., Isacsson, A., Seitner, M. J., Kotthaus, J. P. & Weig, E. M. Energy losses of nanomechanical resonators induced by atomic force microscopy-controlled mechanical impedance mismatching. *Nature Commun.* **5,** 3345 (2014).
11. Tao, Y., Boss, J. M., Moores, B. A. & Degen, C. L. Single crystal diamond nanomechanical resonators with quality factors exceeding one million. *Nature Commun.* **5,** 3638 (2014).
12. Chan, J., Safavi-Naeini, A. H., Hill, J. T., Meenehan, S. & Painter, O. Optimized optomechanical crystal cavity with acoustic radiation shield. *Appl. Phys. Lett.* **101,** 081115 (2012).
13. Anetsberger, G., Rivière, R., Schliesser, A., Arcizet, O. & Kippenberg, T. J. Ultralow-dissipation optomechanical resonators on a chip. *Nature Photon.* **2,** 627–633 (2008).
14. Chan, J. *et al.* Laser cooling of a nanomechanical oscillator into its quantum ground state. *Nature* **478,** 89–92 (2011).
15. Ni, K-K. *et al.* Enhancement of mechanical Q factors by optical trapping. *Phys. Rev. Lett.* **108,** 214302 (2012).
16. Gieseler, J., Deutsch, B., Quidant, R. & Novotny, L. Subkelvin parametric feedback cooling of a laser-trapped nanoparticle. *Phys. Rev. Lett.* **109,** 103603 (2012).
17. Gröblacher, S. *et al.* Demonstration of an ultracold micro-optomechanical oscillator in a cryogenic cavity. *Nature Phys.* **5,** 485–488 (2009).

18. Villanueva, L. G. & Schmid, S. Evidence of surface loss as ubiquitous limiting damping mechanism in SiN micro- and nanomechanical resonators. Preprint at http://arxiv.org/pdf/1405.6115 (2014).
19. Meerwaldt, H. B., Johnston, S. R., van der Zant, H. S. J. & Steele, G. A. Submicrosecond-timescale readout of carbon nanotube mechanical motion. *Appl. Phys. Lett.* **103,** 053121 (2013).
20. Gouttenoire, V. *et al.* Digital and FM demodulation of a doubly clamped single-walled carbon-nanotube oscillator: towards a nanotube cell phone. *Small* **6,** 1060–1065 (2010).
21. Eichler, A. *et al.* Nonlinear damping in mechanical resonators made from carbon nanotubes and graphene. *Nature Nanotech.* **6,** 339–342 (2011).
22. Moser, J. *et al.* Ultrasensitive force detection with a nanotube mechanical resonator. *Nature Nanotech.* **8,** 493–496 (2013).
23. Ganzhorn, M. & Wernsdorfer, W. Dynamics and dissipation induced by single-electron tunneling in carbon nanotube nanoelectromechanical systems. *Phys. Rev. Lett.* **108,** 175502 (2012).
24. Gavartin, E., Verlot, P & Kippenberg, T. J. Stabilization of a linear nanomechanical oscillator to its thermodynamic limit. *Nature Commun.* **4,** 2860 (2013).
25. Fong, K. Y., Pernice, W. H. P. & Tang, H. X. Frequency and phase noise of ultrahigh *Q* silicon nitride nanomechanical resonators. *Phys. Rev. B* **85,** 161410(R) (2012).
26. Villanueva, L. G. *et al.* Surpassing fundamental limits of oscillators using nonlinear resonators. *Phys. Rev. Lett.* **110,** 177208 (2013).
27. Dykman, M. I. & Krivoglaz, M. A. Theory of nonlinear oscillator interacting with a medium. *Sov. Phys. Rev.* **5,** 265–441 (1984).
28. Eichler, A., Moser, J., Dykman, M. I. & Bachtold, A. Symmetry breaking in a mechanical resonator made from a carbon nanotube. *Nature Commun.* **4,** 2843 (2013).
29. Barnard, A. W., Sazonova, V., van der Zande, A. M. & McEuen, P. L. Fluctuation broadening in carbon nanotube resonators. *Proc. Natl Acad. Sci. USA* **109,** 19093 (2012).
30. Longenecker, J. G. *et al.* High-gradient nanomagnets on cantilevers for sensitive detection of nuclear magnetic resonance. *ACS Nano* **6,** 9637–9645 (2012).
31. Laird, E. A., Pei, F., Tang, W., Steele, G. A. & Kouwenhoven, L. P. A high quality factor carbon nanotube mechanical resonator at 39 GHz. *Nano Lett.* **12,** 193–197 (2012).
32. Schneider, B. H., Etaki, S., van der Zant, H. S. J. & Steele, G. A. Coupling carbon nanotube mechanics to a superconducting circuit. *Sci. Rep.* **2,** 599 (2012).
33. Cleland, A. N. & Roukes, M. L. Noise processes in nanomechanical resonators. *J. Appl. Phys.* **92,** 2758–2769 (2002).

Acknowledgements

The authors thank H. Flyvbjerg and S. Nørrelykke for discussions. The authors acknowledge support from the European Union through the ERC-carbonNEMS project (279278), a Marie Curie grant (271938) and the Graphene Flagship, MINECO and FEDER (MAT2012-31338), the Catalan government (AGAUR, SGR), and the US Army Research Office.

Author contributions

J.M. developed the experimental set-up, carried out the measurements and analysed the data. A.E. fabricated the devices. J.G. provided support for the experimental set-up. M.I.D. and A.B. provided support for the analysis. M.I.D. wrote Supplementary Section X. J.M., M.I.D. and A.B. wrote the manuscript, with critical comments from all authors. A.B. and J.M. conceived the experiment. A.B. supervised the work.

Additional information

Supplementary information is available in the online version of the paper. Reprints and permissions information is available online at www.nature.com/reprints. Correspondence and requests for materials should be addressed to A.B.

Competing financial interests

The authors declare no competing financial interests.